

Chirality-induced spin selectivity based on orbital Edelstein effect in an analytically solvable model

Börge Göbel,^{1,*} Lennart Schimpf,¹ and Ingrid Mertig¹

¹*Institut für Physik, Martin-Luther-Universität Halle-Wittenberg, D-06099 Halle (Saale), Germany*

(Dated: February 10, 2025)

Chirality-induced spin selectivity, a phenomenon wherein chiral structures selectively determine the spin polarization of electron currents flowing through the material, has garnered significant attention due to its potential applications in areas such as spintronics, enantioseparation, and catalysis. The underlying physical effect is the Edelstein effect that converts charge to angular momentum but the precise mechanism remains yet to be understood. Here, we introduce the minimal model for explaining the phenomenon based on the orbital Edelstein effect. We consider inter-site contributions to the current-induced orbital angular momentum and reveal the underlying mechanism by analytically calculating the Edelstein susceptibilities in a tight-binding and Boltzmann approach. While the orbital angular momentum is directly generated by the chirality of the crystal, the spin contribution of each spin-split band pair relies on spin-orbit coupling. Using tellurium as an example, we show that the orbital contribution surpasses the spin contribution by orders of magnitude.

Chirality is a geometric property that affects a wide range of scientific fields, from chemistry and biology to physics and material engineering. A structure is chiral if it is distinguishable from its mirror image; it lacks mirror, inversion and roto-inversion symmetries [1]. The structural chirality of molecules like the DNA molecule or crystals like tellurium and selenium [cf. Fig. 1] can affect biochemical properties and even couples to physical observables like the angular momentum which gives rise to an intriguing phenomenon known as chirality-induced spin selectivity (CISS). The chirality of a structure determines the sign of the spin-polarization of electrons moving through it. CISS was first observed in chiral molecules [2]. More recently, this phenomenon has been observed in a broader range of systems, including hybrid organic-inorganic perovskites [3, 4] and chiral crystals like tellurium [1, 5, 6] or CrNb₃S₆ [7, 8].

Despite extensive experimental observations, the underlying physical mechanisms governing CISS remain a topic of active debate. Theoretical explanations are mostly based on the charge-to-spin conversion effect named inverse spin-galvanic effect or Edelstein effect (EE) [9, 10]: Due to a broken inversion symmetry, the spin polarizations of electrons with opposite wave vectors differ which leads to the generation of a spin density once an electric field or currents are applied. The EE typically occurs at interfaces where the broken inversion symmetry gives rise to a Rashba-type spin-orbit coupling [11–13]. In a chiral material, however, the inversion symmetry is innately broken and a collinear effect can occur where the spins are parallel to the wave vector [1, 5, 6, 14, 15] and the theoretically calculated Edelstein susceptibilities indeed depend on the chirality of the structure. However, as was pointed out in Refs. [14, 15], they are an order of magnitude smaller than what was measured experimentally in tellurium [5] pointing towards the existence of important additional contributions.

Recently, several phenomena related to angular momentum have been observed and understood based on the orbital degree of freedom. Orbital-polarized currents, generated by the

orbital Hall effect [16–31] or the orbital EE [32–44] can lead to the generation or transport of orbital angular momentum when currents or electric fields are applied. It has been shown that the orbital EE is sensitive to the chirality of a system as well [33, 34, 38, 39, 42]. We refer to this phenomenon as chirality-induced orbital selectivity (CIOS). When a current flows through a chiral material, it becomes orbital polarized due to a shift of the Fermi surfaces, as visualized in Fig. 2. Once the current enters the electrodes, like Pt which has a considerable spin-orbit coupling (SOC), it is transformed into a spin-polarized current. CIOS is therefore detected effectively as CISS in most experiments, where the orbital contribution is simply scaled by the orbital-to-spin conversion efficiency of the electrode. This contribution occurs additionally to the genuine spin contribution to CISS and could account for the discrepancy of theoretically and experimentally determined CISS efficiencies.

While this has been an important achievement in understanding CISS, so far, the precise mechanism of CIOS is not well understood. Since in most theoretical descriptions, orbital angular momentum is calculated via the hybridization of multiple atomic orbitals at the same atom (atomic-center approximation), the efficiency of CIOS is underestimated and can hardly be understood intuitively because the genuine chiral mechanism is not captured: The orbital angular momentum is mostly generated by the circular motion of electrons among *multiple* atoms forming a helix, like in tellurium. This generates an orbital angular momentum that is always along the current direction for one helix chirality and always opposite for the other (cf. arrows in Fig. 1). Currently, the literature on the orbital Edelstein effect considering such inter-site contributions is scarce. Refs. [33, 34] use the modern formulation of orbital magnetization [45–50] and even make the analogy to a classical solenoid. However, due to the Haldane-like [51] nature of the model [33, 34], requiring multiple independent parameters, the Edelstein susceptibility cannot be calculated analytically. Furthermore, the interpretation based on Weyl points in the three-dimensional Brillouin zone dilutes the intuitive mechanism based on the chirality in real space.

In this paper, we introduce the minimal model for understanding CIOS and CISS. The unit cell of the considered helix consists of only three *s* orbitals and extends periodically

* Correspondence email address: boerge.goebel@physik.uni-halle.de

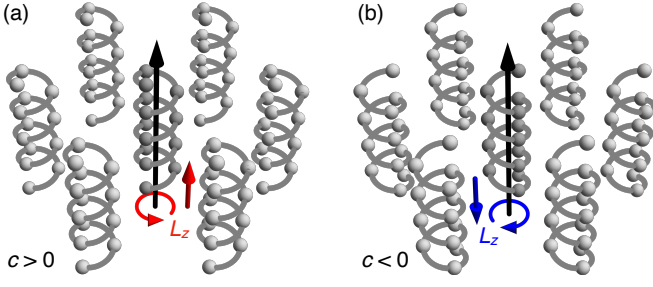


FIG. 1. Chiral helices as in tellurium. (a) Right-handed helix structure characterized by $c > 0$. (b) Left-handed structure characterized by $c < 0$. The black arrow symbolizes the translational motion of electrons along z . It is constrained to a circular motion (red and blue) which generates opposite orbital angular momentum L_z for the two opposite crystal chiralities.

along one dimension. We consider the modern formulation of orbital magnetization for the calculation of the orbital angular momentum to account for inter-site contributions that are crucial for describing the effect in chiral materials properly. Since we can describe this system analytically, we are able to reveal the chiral mechanism of CIOS and CISS based on an orbital EE that is orders of magnitude larger than the spin EE.

Minimal model. The model consists of the most fundamental chiral structure: a helix consisting of 3 atoms akin to the structure in tellurium and resembling its space group $P3_121$ (D_3^4 symmetry) or $P3_221$ (D_3^6 symmetry), depending on the chirality [5]. The three basis atoms positioned at $\mathbf{r}_1 = (0, 0, 0)$, $\mathbf{r}_2 = (a, 0, 1/3 c)$, $\mathbf{r}_3 = (1/2 a, \sqrt{3}/2 a, 2/3 c)$ host a single s orbital and give rise to hopping paths along

$$\begin{aligned} \mathbf{r}_{12} &= (a, 0, 1/3 c), \\ \mathbf{r}_{23} &= (-1/2 a, \sqrt{3}/2 a, 1/3 c), \\ \mathbf{r}_{31} &= (-1/2 a, -\sqrt{3}/2 a, 1/3 c). \end{aligned} \quad (1)$$

The chiral structure is considered periodic along the z direction with a period of c . The sign of c controls the chirality of the helix: right-handed for $c > 0$ and left-handed for $c < 0$, cf. Fig. 1. We also consider periodicity in the xy plane but for simplicity the helices are not coupled by hoppings. This allows us to describe the chiral structure in an effectively one-dimensional Brillouin zone with k_z the only wave vector component that exhibits dispersion.

The tight-binding Hamiltonian requires only a single parameter (nearest-neighbor hopping amplitude t) to capture the chiral mechanism of CIOS

$$H(\mathbf{k}) = -t \begin{pmatrix} 0 & e^{i\mathbf{k}\cdot\mathbf{r}_{12}} & e^{-i\mathbf{k}\cdot\mathbf{r}_{31}} \\ e^{-i\mathbf{k}\cdot\mathbf{r}_{12}} & 0 & e^{i\mathbf{k}\cdot\mathbf{r}_{23}} \\ e^{i\mathbf{k}\cdot\mathbf{r}_{31}} & e^{-i\mathbf{k}\cdot\mathbf{r}_{23}} & 0 \end{pmatrix}. \quad (2)$$

Due to the lack of dispersion along k_x and k_y the band structure along $k \equiv k_z$ reads

$$E_1(k) = -2t \cos\left(k \frac{c}{3}\right), \quad E_{2,3}(k) = E_1\left(k \pm \frac{2\pi}{c}\right).$$

This band structure [Fig. 3(a)] is equivalent to the single band $-2t \cos(k \frac{c}{3})$ characterizing a one-dimensional chain of

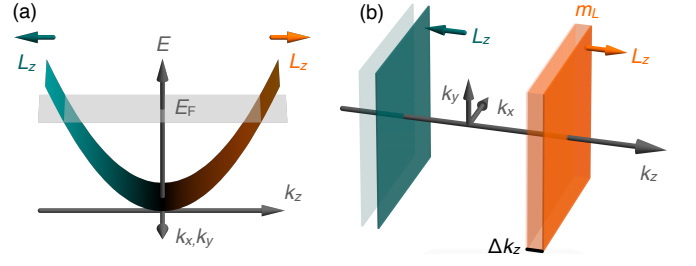


FIG. 2. Orbital Edelstein effect (schematic for $c > 0$). (a) Band structure of free electrons with orbital angular momentum L_z proportional to the group velocity (color). (b) Upon application of an electric field along z , the initial Fermi surfaces (pale) are shifted by Δk_z giving rise to a non-equilibrium orbital magnetic moment m_L .

atoms with lattice constant $c/3$ along z which has been back-folded into the smaller Brillouin zone accounting for the 3 atoms in the unit cell. The eigenvectors $|n\rangle$ along k_z are constant and read

$$|1\rangle = \frac{1}{\sqrt{3}} \begin{pmatrix} 1 \\ 1 \\ 1 \end{pmatrix}, \quad |2,3\rangle = \frac{1}{\sqrt{3}} \begin{pmatrix} 1 \\ -1/2 \pm i\sqrt{3}/2 \\ -1/2 \mp i\sqrt{3}/2 \end{pmatrix}.$$

We calculate the z component of the orbital angular momentum of the n th band based on the modern formulation of orbital magnetization [45–50]

$$\begin{aligned} L_{n,z}(\mathbf{k}) &= i \frac{m_e}{g_L \hbar} \sum_{m \neq n} \frac{1}{E_m(\mathbf{k}) - E_n(\mathbf{k})} \\ &\times [\langle n | \partial H / \partial k_x | m \rangle \langle m | \partial H / \partial k_y | n \rangle - (n \leftrightarrow m)]. \end{aligned} \quad (3)$$

This results in a chirality-dependent orbital angular momentum (opposite for $c > 0$ versus $c < 0$)

$$L_{1,z}(k) = \frac{1}{\sqrt{3}} \frac{m_e}{g_L \hbar} a^2 t \sin\left(k \frac{c}{3}\right), \quad (4)$$

$$L_{2/3,z}(k) = L_{1,z}\left(k \pm \frac{2\pi}{c}\right) \quad (5)$$

that is proportional to the group velocity $v_{n,z}(k) = \frac{1}{\hbar} \frac{\partial E_n}{\partial k_z}$. The fact that the orbital angular momentum is antisymmetric with k , while the band structure is symmetric [cf. also Fig. 3(a)], gives rise to an orbital Edelstein effect, as visualized in Fig. 2.

The collinear orbital Edelstein susceptibility $\chi_z^{L_z}$ relates the applied electric field $\mathbf{E} = E_z \mathbf{e}_z$ and the generated non-equilibrium orbital magnetic moment per unit cell $m_{L_z}^{\text{uc}}$ via $m_{L_z}^{\text{uc}} = \chi_z^{L_z} E_z$. We can calculate $\chi_z^{L_z}$ easily using the Boltzmann transport theory when we assume a constant relaxation time τ

$$\chi_z^{L_z}(E) = \frac{e^2 g_L \tau}{2m_e} \sum_{n,\mathbf{k}} v_{n,z}(k) \cdot L_{n,z}(k) \cdot \delta(E_n(k) - E). \quad (6)$$

This results in

$$\chi_z^{L_z}(E) = \frac{e^2}{2\pi\sqrt{3}\hbar^2} \tau |t| c a^2 \sqrt{1 - \left(\frac{E}{2t}\right)^2}. \quad (7)$$

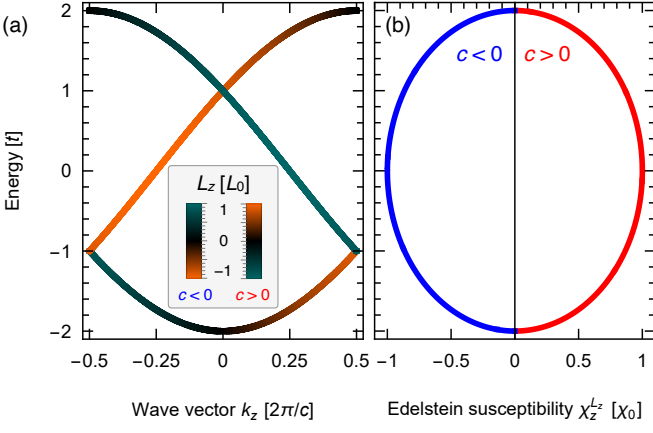


FIG. 3. Chirality-induced orbital selectivity in a chiral system without spin-orbit coupling. (a) Band structure for which the color encodes the orbital angular momentum L_z in units of $L_0 = \frac{1}{\sqrt{3}} \frac{m_e}{g_L \hbar} a^2 t$. (b) Edelstein susceptibility $\chi_z^{L_z}$ in units of $\chi_0 = \frac{e^2}{2\pi\sqrt{3}\hbar^2} \tau |t| c a^2$. The red curve shows the result for the right-handed system ($c > 0$) and the blue curve for the left-handed system ($c < 0$).

The result is proportional to $L_{n,z}^{(k>0)}(E) - L_{n,z}^{(k<0)}(E)$. Therefore, we can easily understand the energy dependence as presented in Fig. 3(b). $\chi_z^{L_z}$ is zero at the band edges due to the zero velocity and is largest in the middle of the band width where the velocity and therefore L_z are largest as well. The orbital Edelstein susceptibility changes sign once the chirality is reversed, due to the linear c dependence [52].

So far, we wanted to make the discussion as general as possible. Now we consider the case of tellurium's s bands that exhibit an almost perfect resemblance of the band structure we have calculated. We use $a = 2.133 \text{ \AA}$, $t = 1.249 \text{ eV}$ [53] and $g_L = 1$ which gives a maximum value for the orbital angular momentum $L_0 = 0.43 \hbar$. For the orbital Edelstein susceptibility we additionally use $c = \pm 6.018 \text{ \AA}$ and assume a typical relaxation time $\tau = 1 \text{ ps}$ which results in an extremum of $\chi_0 = \pm 125.0 \times 10^{-9} \mu_B \text{ m/V}$. The sign depends on the crystal chirality which means the system exhibits an extremely strong yet purely geometrical CIOS that is converted into CISS once measured. $\chi_z^{L_z}$ is orders of magnitude larger than the spin Edelstein susceptibility $\chi_z^{S_z}$ calculated for tellurium in Ref. [6]. In our model $\chi_z^{S_z} = 0$, because spin is not yet considered.

We note that we have restricted our model to one dimension, so that we can solve it analytically. In reality, the individual helices are coupled by van der Waals interactions and dispersion along k_x and k_y emerges. However, especially near the center of the energy range, the Fermi surfaces are sheets that extend throughout the whole $k_x k_y$ plane of the three-dimensional Brillouin zone, similar to the schematics shown in Fig. 2(b). In Figs. S1, S2 in the Supplemental Material [54] we show that the full three-dimensional system is here described well by the quasi-one-dimensional analytical model.

Effect of spin-orbit coupling. After having established the main result of the paper, next, we present how including SOC influences the orbital Edelstein effect and may cause a spin

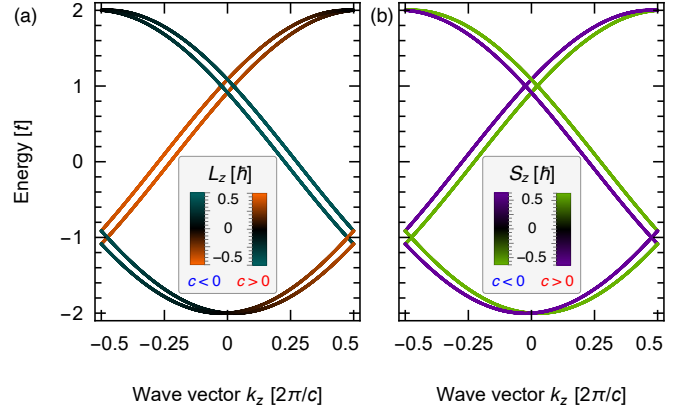


FIG. 4. Band structure of a chiral helix with spin-orbit coupling. (a) The color encodes the orbital angular momentum L_z . (b) The color encodes the spin S_z . Parameters correspond to tellurium with exaggerated spin-orbit coupling $\lambda = 0.05t$.

Edelstein effect as well; two effects relying on distinct mechanisms. First, we make the Hamiltonian spin dependent. Without SOC, all bands are now doubly degenerate but the orbital angular momentum always has the same value for the two uncoupled spin-subsystems. Therefore, the orbital Edelstein susceptibility $\chi_z^{L_z}(E)$ is simply increased by a factor of 2 to a maximum of $250.0 \times 10^{-9} \mu_B \text{ m/V}$. The spin Edelstein susceptibility $\chi_z^{S_z}(E) = 0$ due to Kramer's degeneracy.

SOC is included akin to the Kane-Mele model [55], that can be written in second quantization

$$i\lambda \sum_{\langle i,j \rangle} \nu_{ij} c_i^\dagger \sigma_z c_j. \quad (8)$$

Here c_i^\dagger and c_j are the creation and annihilation operators at sites i, j . $\nu_{ij} = \pm 1$ accounts for the hopping path along the helix: $+1$ for a counter-clockwise rotation and -1 for a clockwise rotation, so $+\text{sign}(c)$ for hopping along $+z$ and $-\text{sign}(c)$ for hopping along $-z$. The resulting band structure [Figs. 4(a,b)] is

$$\begin{aligned} E_{1}^{\uparrow\downarrow}(k) &= -2t \cos\left(k \frac{c}{3}\right) \mp 2\lambda \sin\left(k \frac{c}{3}\right), \\ E_{2/3}^{\uparrow\downarrow}(k) &= E_{1}^{\uparrow\downarrow}\left(k \pm \frac{2\pi}{c}\right). \end{aligned} \quad (9)$$

Note the sign change of the SOC term for $c > 0$ and $c < 0$: The sine function comes from adding the two hopping terms along $\pm c e_z$ where the upwards hopping path along the helix is rotating oppositely to the downwards hopping path: $i[\exp(ick_z) - \exp(-ick_z)]$. Furthermore, it depends on the spin-orientation. Close to the Γ point the SOC-induced term is $\mp 2\lambda k_z c/3$, a term that has been derived in Ref. [56] as well.

The Hamiltonian is separated into spin-up and spin-down blocks meaning that all bands are $\pm 100\%$ spin polarized $S_{n,z}^{\uparrow\downarrow}(k) = \pm \frac{\hbar}{2}$ [color in Fig. 4(b)]. This makes the system under consideration similar to a Dresselhaus system [57], where the structural chirality breaks the inversion symmetry, but in one dimension. The spin is (anti-) parallel to k ; a feature well

known from the Fermi surface of tellurium so the expected spin Edelstein effect is collinear [1, 5, 6, 14, 15] meaning that electric field and generated magnetic moment are collinear.

Conversely, the orbital angular momenta of the two bands of each spin-split band pair are almost the same [Fig. 4(a)]. They are affected in a similar way as the band structure

$$\begin{aligned} L_{1,z}^{\uparrow\downarrow}(k) &= \frac{1}{\sqrt{3}} \frac{m_e}{g_L \hbar} a^2 \left[t \sin\left(k \frac{c}{3}\right) \mp \lambda \cos\left(k \frac{c}{3}\right) \right], \\ L_{2/3,z}^{\uparrow\downarrow}(k) &= L_{1,z}^{\uparrow\downarrow}\left(k \pm \frac{2\pi}{c}\right) \end{aligned} \quad (10)$$

and so the orbital Edelstein susceptibility is merely rescaled due to the new bandwidth $\tilde{t}_\lambda = t\sqrt{1 + (\lambda/t)^2}$

$$\chi_z^{L_z}(E) = \frac{e^2}{\pi\sqrt{3}\hbar^2} \tau c a^2 |\tilde{t}_\lambda| \sqrt{1 - \left(\frac{E}{2\tilde{t}_\lambda}\right)^2}. \quad (11)$$

Even if the SOC were 5% of the hopping amplitude $\lambda = 0.05t$, the maximum of the orbital Edelstein susceptibility changes by only 0.125%. This highlights that the orbital Edelstein effect is not governed by SOC but purely by the chiral structure of the helices.

The contributions of the inner and outer bands to the spin Edelstein susceptibility cancel, $\chi_z^{S_z} = 0$. In Fig. S3 in the Supplemental Material [54], we show that once a spin EE emerges, e. g. by considering a k -dependent relaxation time, it is proportional to spin-orbit coupling and orders of magnitude smaller than the orbital EE.

Discussion. We have analytically shown that the current-induced selectivity of spin and orbital angular momentum in chiral materials like selenium and tellurium follow fundamentally different mechanisms. The orbital contributions from bands with opposite spin directions add up and the effect occurs even without SOC. The spin EE of both bands (almost) cancels and scales with SOC making it a less efficient mechanism. As mentioned in the introduction, in an experiment, the orbital-polarized currents will be converted into spin-polarized currents upon passing through the detecting electrode so the CIOS will effectively be detected as CISS. Our work fills the gap between large experimentally observed signals and the Edelstein signals that were calculated before based on only the spin EE or on the orbital EE effect in atomic-center approximation.

Effective single-band description. Lastly, we want to compare the quantum mechanical results with a classical description using constraints. If an electron moves along the helix, it carries out a net motion along z superimposed by a periodic motion along the edges of a triangle in the xy plane. The latter generates an orbital angular momentum $L_z = m_e \frac{a}{2\sqrt{3}} v_{xy}$ with respect to the center of this triangle. The geometry introduces a constraint of the periodic and translational motion: the in-plane velocity along the sides of the triangle v_{xy} is proportional to the velocity along the periodic direction v_z , so $v_{xy} = v_z \cdot 3a/c$. This means, the orbital angular momentum and the velocity along z are proportional to each other $L_z^{\text{classical}} = m_e \frac{\sqrt{3}a^2}{2c} v_z$ which is a signature of the system's chirality.

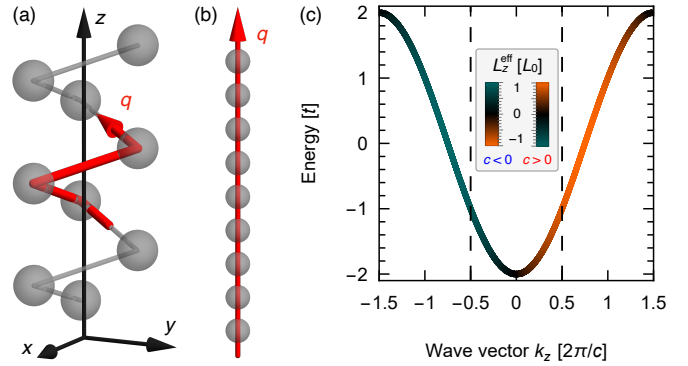


FIG. 5. Effective 1-band model. (a) Helix structure for $c > 0$ with generalized coordinate q (red). (b) Structure along this new effective coordinate. (c) Band structure with effective orbital angular momentum (color). The dashed line indicates the smaller Brillouin zone corresponding to a chain with 3 atoms in the unit cell.

If we carry over this result to the quantum mechanical tight-binding model, we can effectively describe the system by a single band (or band-pair when spin is considered). The initial system [Fig. 5(a)] with a generalized coordinate q is mapped to a 1-dimensional chain along z with lattice constant $c/3$ [Fig. 5(b)] and the Brillouin zone is now three times as large along k_z as before. This mapping is possible because the local environment of all three basis atoms in the helix is equivalent: We can go from one atom to another by rotation and translation.

The 1-dimensional chain by itself is not chiral anymore and motion along the chain would not give rise to an orbital angular momentum. However, we can account for the periodic in-plane motion by introducing an effective orbital angular momentum operator L_z^{eff} . It is derived by replacing the Hamilton function \mathcal{H} with the Hamilton operator H^{eff} for the calculation of the velocity along the helix direction $v_z = \frac{\partial \mathcal{H}}{\partial p_z} \rightarrow v_z = \frac{1}{\hbar} \frac{\partial H^{\text{eff}}}{\partial k_z}$ leading to

$$L_z^{\text{eff}} = m_e \frac{\sqrt{3}a^2}{2c\hbar} \frac{\partial H^{\text{eff}}}{\partial k_z}. \quad (12)$$

Together with this operator, the effective Hamiltonian

$$H^{\text{eff}}(k_z) = -2t \cos(k_z c/3) \sigma_0 - 2\lambda \sin(k_z c/3) \sigma_z \quad (13)$$

gives rise to the exact same Edelstein susceptibilities $\chi_z^{L_z}(E)$ and $\chi_z^{S_z}(E)$ as the full model considered before, in agreement with the Ehrenfest theorem. This is because $E(k_z)$, $L_z(k_z)$ and $S_z(k_z)$ are the same as before only that the system is now described in a larger Brillouin zone [Fig. 5(c)]. This effective 2-band description (or 1-band description without spin) shows that a semi-classical explanation of CIOS is applicable and allows us to understand even easier why the orbital EE is much larger than the spin EE.

Note, that this analogy is only truly valid when the helices are not coupled by hopping terms so that $L_z \propto v_z$. However, as we have shown in Fig. S1 in the Supplemental Material [54], the analytical results even agree well with the numerical calculations based on a full three-dimensional description.

Acknowledgements — This work was supported by the EIC Pathfinder OPEN grant 101129641 “Orbital Engineering for Innovative Electronics”. B.G. and L.S. performed calculations. B.G. did the analytical derivations, prepared the figures

and planned and supervised the project. All authors discussed the results. B.G. wrote the manuscript with significant inputs from all authors. I.M. provided the funding.

-
- [1] T. Furukawa, Y. Watanabe, N. Ogasawara, K. Kobayashi, and T. Itou, Current-induced magnetization caused by crystal chirality in nonmagnetic elemental tellurium, *Phys. Rev. Res.* **3**, 023111 (2021).
- [2] K. Ray, S. Ananthavel, D. Waldeck, and R. Naaman, Asymmetric scattering of polarized electrons by organized organic films of chiral molecules, *Science* **283**, 814 (1999).
- [3] H. Lu, J. Wang, C. Xiao, X. Pan, X. Chen, R. Brunecy, J. J. Berry, K. Zhu, M. C. Beard, and Z. V. Vardeny, Spin-dependent charge transport through 2d chiral hybrid lead-iodide perovskites, *Science Advances* **5**, eaay0571 (2019).
- [4] Z. Huang, B. P. Bloom, X. Ni, Z. N. Georgieva, M. Marciessy, E. Vetter, F. Liu, D. H. Waldeck, and D. Sun, Magneto-optical detection of photoinduced magnetism via chirality-induced spin selectivity in 2d chiral hybrid organic–inorganic perovskites, *ACS Nano* **14**, 10370 (2020).
- [5] T. Furukawa, Y. Shimokawa, K. Kobayashi, and T. Itou, Observation of current-induced bulk magnetization in elemental tellurium, *Nature Comms.* **8**, 954 (2017).
- [6] F. Calavalle, M. Suárez-Rodríguez, B. Martín-García, A. Johansson, D. C. Vaz, H. Yang, I. V. Maznichenko, S. Ostanin, A. Mateo-Alonso, A. Chuvilin, *et al.*, Gate-tunable and chirality-dependent charge-to-spin conversion in tellurium nanowires, *Nature Mater.* **21**, 526 (2022).
- [7] A. Inui, R. Aoki, Y. Nishiue, K. Shiota, Y. Kousaka, H. Shishido, D. Hirobe, M. Suda, J.-i. Ohe, J.-i. Kishine, *et al.*, Chirality-induced spin-polarized state of a chiral crystal CrNb₃S₆, *Phys. Rev. Lett.* **124**, 166602 (2020).
- [8] Y. Nabei, D. Hirobe, Y. Shimamoto, K. Shiota, A. Inui, Y. Kousaka, Y. Togawa, and H. M. Yamamoto, Current-induced bulk magnetization of a chiral crystal CrNb₃S₆, *Appl. Phys. Lett.* **117**, 052408 (2020).
- [9] A. Aronov and Y. B. Lyanda-Geller, Nuclear electric resonance and orientation of carrier spins by an electric field, *Soviet Journal of Experimental and Theoretical Physics Letters* **50**, 431 (1989).
- [10] V. M. Edelstein, Spin polarization of conduction electrons induced by electric current in two-dimensional asymmetric electron systems, *Solid State Communications* **73**, 233 (1990).
- [11] E. Rashba, Properties of semiconductors with an extremum loop, *Sov. Phys.-Solid State* **2**, 1109 (1960).
- [12] Y. A. Bychkov and É. I. Rashba, Properties of a 2d electron gas with lifted spectral degeneracy, *JETP Lett* **39**, 78 (1984).
- [13] Y. A. Bychkov and E. I. Rashba, Oscillatory effects and the magnetic susceptibility of carriers in inversion layers, *Journal of physics C: Solid state physics* **17**, 6039 (1984).
- [14] A. Roy, F. T. Cerasoli, A. Jayaraj, K. Tenzin, M. B. Nardelli, and J. Sławińska, Long-range current-induced spin accumulation in chiral crystals, *npj Computational Materials* **8**, 243 (2022).
- [15] J. Sławińska, Spin selectivity in elemental tellurium and other chiral materials, *Appl. Phys. Lett.* **123**, 240504 (2023).
- [16] S. Zhang and Z. Yang, Intrinsic spin and orbital angular momentum Hall effect, *Phys. Rev. Lett.* **94**, 066602 (2005).
- [17] B. A. Bernevig, T. L. Hughes, and S.-C. Zhang, Orbitoronics: The intrinsic orbital current in *p*-doped silicon, *Phys. Rev. Lett.* **95**, 066601 (2005).
- [18] H. Kontani, T. Tanaka, D. Hirashima, K. Yamada, and J. Inoue, Giant intrinsic spin and orbital Hall effects in Sr₂MO₄ (*M*= Ru, Rh, Mo), *Phys. Rev. Lett.* **100**, 096601 (2008).
- [19] T. Tanaka, H. Kontani, M. Naito, T. Naito, D. S. Hirashima, K. Yamada, and J. Inoue, Intrinsic spin Hall effect and orbital Hall effect in 4*d* and 5*d* transition metals, *Phys. Rev. B* **77**, 165117 (2008).
- [20] H. Kontani, T. Tanaka, D. Hirashima, K. Yamada, and J. Inoue, Giant orbital Hall effect in transition metals: Origin of large spin and anomalous Hall effects, *Phys. Rev. Lett.* **102**, 016601 (2009).
- [21] D. Go, D. Jo, C. Kim, and H.-W. Lee, Intrinsic spin and orbital Hall effects from orbital texture, *Phys. Rev. Lett.* **121**, 086602 (2018).
- [22] A. Pezo, D. G. Ovalle, and A. Manchon, Orbital Hall effect in crystals: Interatomic versus intra-atomic contributions, *Phys. Rev. B* **106**, 104414 (2022).
- [23] L. M. Canonico, T. P. Cysne, A. Molina-Sanchez, R. Muniz, and T. G. Rappoport, Orbital Hall insulating phase in transition metal dichalcogenide monolayers, *Phys. Rev. B* **101**, 161409 (2020).
- [24] T. P. Cysne, S. Bhowal, G. Vignale, and T. G. Rappoport, Orbital Hall effect in bilayer transition metal dichalcogenides: From the intra-atomic approximation to the Bloch states orbital magnetic moment approach, *Phys. Rev. B* **105**, 195421 (2022).
- [25] L. Salemi and P. M. Oppeneer, Theory of magnetic spin and orbital Hall and Nernst effects in bulk ferromagnets, *Phys. Rev. B* **106**, 024410 (2022).
- [26] O. Busch, I. Mertig, and B. Göbel, Orbital Hall effect and orbital edge states caused by *s* electrons, *Phys. Rev. Res.* **5**, 043052 (2023).
- [27] Y.-G. Choi, D. Jo, K.-H. Ko, D. Go, K.-H. Kim, H. G. Park, C. Kim, B.-C. Min, G.-M. Choi, and H.-W. Lee, Observation of the orbital Hall effect in a light metal Ti, *Nature* **619**, 52 (2023).
- [28] I. Lyalin, S. Alikhah, M. Berritta, P. M. Oppeneer, and R. K. Kawakami, Magneto-optical detection of the orbital Hall effect in chromium, *Phys. Rev. Lett.* **131**, 156702 (2023).
- [29] O. Busch, F. Ziolkowski, B. Göbel, I. Mertig, and J. Henk, Ultrafast orbital Hall effect in metallic nanoribbons, *Phys. Rev. Res.* **6**, 013208 (2024).
- [30] B. Göbel and I. Mertig, Orbital Hall Effect Accompanying Quantum Hall Effect: Landau Levels Cause Orbital Polarized Edge Currents, *Phys. Rev. Lett.* **133**, 146301 (2024).
- [31] B. Göbel, L. Schimpf, and I. Mertig, Topological orbital Hall effect caused by skyrmions and antiferromagnetic skyrmions, *Communications Physics* **8**, 17 (2025).
- [32] L. Levitov, Y. V. Nazarov, and G. Eliashberg, Magnetoelectric effects in conductors with mirror isomer symmetry, *Soviet Journal of Experimental and Theoretical Physics* **61**, 133 (1985).
- [33] T. Yoda, T. Yokoyama, and S. Murakami, Current-induced orbital and spin magnetizations in crystals with helical structure, *Scientific Reports* **5**, 12024 (2015).

- [34] T. Yoda, T. Yokoyama, and S. Murakami, Orbital Edelstein effect as a condensed-matter analog of solenoids, *Nano Lett.* **18**, 916 (2018).
- [35] D. Go, J.-P. Hanke, P. M. Buhl, F. Freimuth, G. Bihlmayer, H.-W. Lee, Y. Mokrousov, and S. Blügel, Toward surface orbitronics: giant orbital magnetism from the orbital Rashba effect at the surface of *sp*-metals, *Scientific Reports* **7**, 46742 (2017).
- [36] L. Salemi, M. Berritta, A. K. Nandy, and P. M. Oppeneer, Orbitaly dominated Rashba-Edelstein effect in noncentrosymmetric antiferromagnets, *Nature Comms.* **10**, 5381 (2019).
- [37] A. Johansson, B. Göbel, J. Henk, M. Bibes, and I. Mertig, Spin and orbital Edelstein effects in a two-dimensional electron gas: Theory and application to SrTiO₃ interfaces, *Phys. Rev. Res.* **3**, 013275 (2021).
- [38] Y. Liu, J. Xiao, J. Koo, and B. Yan, Chirality-driven topological electronic structure of DNA-like materials, *Nature Mater.* **20**, 638 (2021).
- [39] B. Kim, D. Shin, S. Namgung, N. Park, K.-W. Kim, and J. Kim, Optoelectronic manifestation of orbital angular momentum driven by chiral hopping in helical se chains, *ACS Nano* **17**, 18873 (2023).
- [40] A. El Hamdi, J.-Y. Chauleau, M. Boselli, C. Thibault, C. Gorini, A. Smogunov, C. Barreateau, S. Gariglio, J.-M. Triscone, and M. Viret, Observation of the orbital inverse Rashba-Edelstein effect, *Nature Phys.* **19**, 1855 (2023).
- [41] S. Leiva-Montecinos, J. Henk, I. Mertig, and A. Johansson, Spin and orbital Edelstein effect in a bilayer system with Rashba interaction, *Phys. Rev. Res.* **5**, 043294 (2023).
- [42] K. Hagiwara, Y.-J. Chen, D. Go, X. L. Tan, S. Grytsiuk, K.-H. O. Yang, G.-J. Shu, J. Chien, Y.-H. Shen, X.-L. Huang, *et al.*, Orbital topology of chiral crystals for orbitronics, arXiv preprint arXiv:2410.20607 [10.48550/arXiv.2410.20607](https://arxiv.org/abs/2410.20607) (2024).
- [43] A. Johansson, Theory of spin and orbital Edelstein effects, *J. Phys.: Condens. Matt.* **36**, 423002 (2024).
- [44] J. M. Lee, M. J. Park, and H.-W. Lee, Orbital Edelstein effect of electronic itinerant orbital motion at edges, *Phys. Rev. B* **110**, 134436 (2024).
- [45] M.-C. Chang and Q. Niu, Berry phase, hyperorbits, and the Hofstadter spectrum: Semiclassical dynamics in magnetic Bloch bands, *Phys. Rev. B* **53**, 7010 (1996).
- [46] D. Xiao, J. Shi, and Q. Niu, Berry phase correction to electron density of states in solids, *Phys. Rev. Lett.* **95**, 137204 (2005).
- [47] T. Thonhauser, D. Ceresoli, D. Vanderbilt, and R. Resta, Orbital magnetization in periodic insulators, *Phys. Rev. Lett.* **95**, 137205 (2005).
- [48] D. Ceresoli, T. Thonhauser, D. Vanderbilt, and R. Resta, Orbital magnetization in crystalline solids: Multi-band insulators, Chern insulators, and metals, *Phys. Rev. B* **74**, 024408 (2006).
- [49] A. Raoux, F. Piéchon, J.-N. Fuchs, and G. Montambaux, Orbital magnetism in coupled-bands models, *Phys. Rev. B* **91**, 085120 (2015).
- [50] B. Göbel, A. Mook, J. Henk, and I. Mertig, Magnetoelectric effect and orbital magnetization in skyrmion crystals: Detection and characterization of skyrmions, *Phys. Rev. B* **99**, 060406 (2019).
- [51] F. D. M. Haldane, Model for a quantum Hall effect without landau levels: Condensed-matter realization of the "parity anomaly", *Phys. Rev. Lett.* **61**, 2015 (1988).
- [52] Note that increasing the helix period c would lead to a decreased hopping amplitude t .
- [53] J. Li, A. Ciani, J. Gayles, D. Papaconstantopoulos, N. Kioussis, C. Grein, and F. Aqariden, Non-orthogonal tight-binding model for tellurium and selenium, *Philosophical Magazine* **93**, 3216 (2013).
- [54] See Supplemental Material at [URL] for a comparison with the full three-dimensional system and for additional calculations of the orbital and spin Edelstein susceptibilities with a k -dependent relaxation time.
- [55] C. L. Kane and E. J. Mele, Z_2 topological order and the quantum spin Hall effect, *Phys. Rev. Lett.* **95**, 146802 (2005).
- [56] Z.-G. Yu, Chirality-induced spin-orbit coupling, spin transport, and natural optical activity in hybrid organic-inorganic perovskites, *The Journal of Physical Chemistry Letters* **11**, 8638 (2020).
- [57] G. Dresselhaus, Spin-orbit coupling effects in zinc blende structures, *Phys. Rev.* **100**, 580 (1955).